Hysteresis of soil moisture spatial heterogeneity and the "homogenizing" effect of vegetation

Valeriy Y. Ivanov,[1] Simone Fatichi,[1,2] G. Darrel Jenerette,[3] Javier F. Espeleta,[4] Peter A. Troch,[4,5] and Travis E. Huxman[4,6]

Received 3 September 2009; revised 25 January 2010; accepted 19 March 2010; published 16 September 2010.

[1] By partitioning mass and energy fluxes, soil moisture exerts a fundamental control on basin hydrological response. Using the design characteristics of the Biosphere 2 hillslope experiment, this study investigates aspects of soil moisture spatial and temporal variability in a zero-order catchment of a semiarid climate. The hydrological response of the domain exhibits a particular structure, which depends on whether topography-induced subsurface stormflow is triggered. The occurrence of the latter is conditioned by topography, soil depth, and pre-storm spatial distribution of moisture. As a result, a non-unique behavior of soil moisture spatial heterogeneity emerges, manifested through a hysteretic dependence of variability metrics on mean water content. Further, it is argued that vegetation dynamics impose a "homogenizing" effect on pre-storm moisture states, decreasing the likelihood that a rainfall event will result in topographic redistribution of soil water. Consequently, post-rainfall soil moisture dynamics associated with the effect of topography that could lead to the enhancement of spatial heterogeneity are suppressed; a potential "attractor" of catchment states emerges. The study thus proposes several hypotheses that will be testable within the framework of long-term hillslope experiments.

Citation: Ivanov, V. Y., S. Fatichi, G. D. Jenerette, J. F. Espeleta, P. A. Troch, and T. E. Huxman (2010), Hysteresis of soil moisture spatial heterogeneity and the "homogenizing" effect of vegetation, *Water Resour. Res.*, *46*, W09521, doi:10.1029/2009WR008611.

1. Introduction

[2] There is a growing need to characterize soil moisture variability across a range of spatial and temporal scales because of the importance of its implications for both theoretical and practical applications [e.g., *Entekhabi and Rodriguez-Iturbe*, 1994; *Western et al.*, 2004; *Famiglietti et al.*, 2008; *Vivoni et al.*, 2008]. Several modeling and field studies have been carried out to address the properties of soil water spatiotemporal variability [e.g., *Albertson and Montaldo*, 2003; *Cosh et al.*, 2004; *Teuling and Troch*, 2005; *Teuling et al.*, 2007; *Famiglietti et al.*, 2008; *Cosh et al.*, 2008; *Vivoni et al.*, 2008] but conclusions generally vary. For example, several studies have argued that the coefficient of spatial variation of soil moisture, C_v, is inversely related to the mean soil moisture, $\overline{\theta}$, reflecting the notion that moisture is spatially more variable at the drier end of the feasible range relative to the mean value [*Famiglietti et al.*, 1999; *Kumar*, 2004; *Choi et al.*, 2007; *Famiglietti et al.*, 2008, and references therein]. Different patterns have been argued in other studies that identified more complex modes of soil moisture variability depending on climate, vegetation and soil types [e.g., *Albertson and Montaldo*, 2003; *Teuling and Troch*, 2005]. For example, in an effort to explain observations on spatial variability of shallow soil moisture, *Lawrence and Hornberger* [2007] propose various contributing factors in terms of soil properties that are argued to be dominant over certain ranges of moisture contents corresponding to different climates. The resulting curves of soil moisture variance, σ^2, as a function of the mean value, $\sigma^2(\overline{\theta})$, are then expressed by a convex parabolic shape: σ^2 decreases with decreasing $\overline{\theta}$ in arid-semiarid climates and with increasing $\overline{\theta}$ in humid climates, reaching a peak in the mid-range of feasible soil moisture range. *Choi et al.* [2007] presented numerous data sets that are unlikely to be explained only by the hypothesis of *Lawrence and Hornberger* [2007]. Furthermore, *Teuling et al.* [2007] argued that climate variability can lead to non-uniqueness of the $\sigma(\overline{\theta})$ curves. What appears then to be the only possible generalization is that as the mean soil moisture approaches limiting states, at the dry or wet ends, the absolute spatial variability of soil moisture becomes smaller [e.g., *Lawrence and Hornberger*, 2007]; between these bounds, however, the $\sigma^2(\overline{\theta})$ or $C_v(\overline{\theta})$ relationships can be non-unique and depend on climate, soil, vegetation, topography, and antecedent states [e.g., *Albertson and Montaldo*, 2003; *Teuling and Troch*, 2005; *Teuling et al.*, 2007; *Lawrence and Hornberger*, 2007].

[3] This work addresses aspects of soil moisture spatial variability as affected by topography and vegetation in a

[1]Department of Civil and Environmental Engineering, University of Michigan, Ann Arbor, Michigan, USA.
[2]Department of Civil and Environmental Engineering, University of Florence, Florence, Italy.
[3]Department of Botany and Plant Sciences, University of California, Riverside, California, USA.
[4]Biosphere 2, University of Arizona, Tucson, Arizona, USA.
[5]Department of Hydrology and Water Resources, University of Arizona, Tucson, Arizona, USA.
[6]Department of Ecology and Evolutionary Biology, University of Arizona, Tucson, Arizona, USA.

0043-1397/10/2009WR008611

semiarid climate. A zero-order basin, i.e., a topographic form that has an unchanellized hollow that may sporadically drain [e.g., *Tsuboyama et al.*, 2000], is used as a study test bed. The overall slope of the domain surface is ~17.5%, i.e., the 10 degree slope [*Hopp et al.*, 2009]. Note that most previous studies were conducted on relatively flat meadows with a range of slopes less than 1% (WC11, WC13 in work by *Choi et al.* [2007]), 3–5% (Big Meadows in work by *Lawrence and Hornberger* [2007]), ~4% and ~6% Louvain-la-Neuve field and Tarrawarra catchment, respectively, in work by *Teuling and Troch* [2005]). Note also the interchangeable usage of the terms "zero-order basin" and "hillslope" in this manuscript, as the subtle differences between the two can be neglected in the context of the discussion. Specifically, this study analyzes the pattern of the $C_v(\bar{\theta})$ relationship, pointing to the existence of local and non-local controls in the system [e.g., *Grayson et al.*, 1997]. Detailed numerical modeling was carried out as a complementary effort to the pre-construction evaluation exercise of the long-term Biosphere 2 project [*Hopp et al.*, 2009]. Simulations were conducted with a physically-based hydrological model coupled to a mechanistic model of vegetation dynamics. Both had been previously verified using detailed data for the Lucky Hills research site [e.g., *Scott et al.*, 2000] located in the USDA-ARS Walnut Gulch Experimental Watershed, Arizona, USA [e.g., *Emmerich and Verdugo*, 2008; *Renard et al.*, 2008]. The primary emphasis of the experimental design and analysis was the mechanistic interpretation of the $C_v(\bar{\theta})$ relationship in a vegetated semiarid system at various stages of the hydrological response. Furthermore, when integrated over long-term scales, a characteristic role of vegetation function on soil moisture spatial variability was discovered. The study thus proposes several research hypotheses that will be testable within the framework of long term experimental hillslopes, such as the Biosphere 2 project [*Hopp et al.*, 2009].

[4] The manuscript material is organized as following. First, the overall design and methodology of numerical experiments are presented. In what follows, the non-uniqueness in the relationship between the mean domain soil moisture and the coefficient of variation of depth-integrated soil water is demonstrated by using the results of the long-term simulations. The underlying effect of hysteresis of soil moisture spatial organization is then demonstrated and examined in a series of experiments that simulate dry-down events resulting from a single input of rain. In order to help understand the results of these experiments, the temporal evolution of the coefficient of variation of depth-integrated soil moisture is examined using two characteristic examples. A statistical method is then employed to identify the likeliest (in probabilistic terms) processes that are the responsible for the evolution of spatial heterogeneity of soil moisture in these examples. Finally, the long-term impact of vegetation on soil moisture variability is discussed and compared to the scenario in which bare soil was imposed as the state of the domain surface.

2. Design of Numerical Experiments

[5] Biosphere 2 is a large-scale Earth science facility near Tucson (AZ, USA) presenting a variety of opportunities for in situ experiments of environmental processes in a controlled physical environment [*Huxman et al.*, 2009]. Current plans involve the construction and instrumentation of three experimental hillslopes that will be used for studying the interactions among hydrological, ecological, and geochemical processes. The hillslopes will be composed of loamy sand [*Hopp et al.*, 2009], each measuring 30 m × 15 m × 1 m in geometric dimensions. The corresponding hydraulic parameters for the van Genuchten-Mualem soil hydraulic model [*van Genuchten*, 1980] were estimated from the soil catalog of *Carsel and Parrish* [1988] with the saturated hydraulic conductivity K_s = 146 [mm hr^{-1}], the saturation moisture content θ_s = 0.41 [mm^3 mm^{-3}], the residual moisture content θ_r = 0.057 [mm^3 mm^{-3}], and parameters α = −0.0124 [mm^{-1}] and n = 2.28. These parameter values were used in all modeling experiments described below with soil assumed to be isotropic. Further information on science-driven design criteria and specifics of the anticipated hydrological and geochemical behavior are provided by *Hopp et al.* [2009] and *Dontsova et al.* [2009].

[6] The experimental framework uses the design characteristics of the Biosphere 2 facility with the assumption that this controlled environment will eventually offer the feasibility of testing hypotheses drawn in this study. A modeling approach is employed and a detailed ecohydrology model is used to carry out these "hypothesis-generating" numerical experiments. A fully coupled dynamic model of vegetation-hydrology interactions known as tRIBS+VEGGIE is used, detailed earlier by *Ivanov et al.* [2008a]. In short, the model mimics principal water and energy processes over the complex topography of a river basin and links them to the essential plant biochemical processes and phenology. The model features a modular structure allowing for a fairly straightforward substitution of components describing the physics of individual processes. Major recent model developments involved adaptation of the quasi-three-dimensional framework of subsurface flow module to the mixed formulation of the Richards' equation [*Hillel*, 1980; *Celia et al.*, 1990], allowing for the computation of groundwater dynamics; implementation of a new scheme of atmospheric resistance in the surface boundary layer [*Mascart et al.*, 1995], allowing for a seamless incorporation of the relative effects of buoyancy and mechanical turbulence; re-formulation of the soil resistance to surface evaporation based on the numerically defined maximum soil exfiltration flux rate; and implementation of *Leuning* [1995] stomatal aperture model exhibiting more robust properties for arid environments. The general consistency of the model behavior at the plot scale has been previously confirmed for generic annual C_4 grasses [*Ivanov et al.*, 2008b] and a mixture of deciduous and evergreen shrubs [*Ivanov et al.*, 2008c] using the long-term observations of energy fluxes, multiple-depth soil moisture series, and in situ and remote sensing measurements of biomass. *Bisht et al.* [2008] and *Sivandran et al.* [2008] have demonstrated satisfactory performance of the model in reproducing seasonality characteristics of vegetation at larger, watershed scales.

[7] The Biosphere 2 domain [*Hopp et al.*, 2009] was discretized at 1 m by 1 m in the horizontal plane and resolved on eighteen mesh nodes in the vertical plane, with spacing varying between 20 mm (soil top) and 80 mm (soil bottom) at each location. Flux (Neumann) boundary condition was specified at the surface of the domain, allowing for infiltration, runoff, and exfiltration fluxes. The downslope boundary of the hillslope was approximated as a seepage face, where

Table 1. Parameters of Vegetation Biochemical, Allocation, Phenology, and Water Uptake Processes for a Generic Evergreen Shrub[a]

Parameter	Unit	Value
$V_{\max 25}$	[μmol CO_2 m^{-2} s^{-1}]	30.0
K	[–]	0.5
m	[–]	9
b	[μmol m^{-2} s^{-1}]	10,000
$\epsilon_{3,4}$	[μmol CO_2 μ mol $phot^{-1}$]	0.08
r_{sapw}	[g C g C^{-1} s^{-1}]	15.0×10^{-10}
r_{root}	[g C g C^{-1} s^{-1}]	80×10^{-10}
ω_{grw}	[–]	0.25
d_{leaf}	[$year^{-1}$]	1.5
d_{sapw}	[$year^{-1}$]	5.0
d_{root}	[$year^{-1}$]	1.0
e_{leaf}	[–]	0.35
e_{sapw}	[–]	0.10
e_{root}	[–]	0.55
$\tau_{\Lambda(NIR)}^{leaf}$	[–]	0.05
$\tau_{\Lambda(NIR,\ VIS)}^{stem}$	[–]	10^{-9}
S_{la}	[m^2 leaf kg C^{-1}]	0.10
$\gamma_{W\max}$	[day^{-1}]	1/150
b_W	[–]	4.0
$\gamma_{C\max}$	[day^{-1}]	1/200
b_C	[–]	2.0
T_{cold}	[°C]	6.0
ϖ	[–]	0.05
ε_s	[–]	120.0
ξ	[–]	2.67
f_{LS}	[–]	0.30
$\overline{T}_{soil}$	[°C]	2.0
D_0	[Pa]	2200

[a]The parameters, notation, and units are defined by *Ivanov et al.* [2008a]. Biophysical and interception parameters are the same as for the "broadleaf deciduous tree" plant functional type in Table 2 of *Ivanov et al.* [2008a] with the exception of τ_{Λ}^{leaf} (NIR), τ_{Λ}^{stem} (both VIS and NIR spectral bands), and S_{la}. The new values of these parameters are provided in this table. The parameters D_{LH}^{C}, $\Delta\ T_{\min,\ Fav}$, $f_{C,\ init}$, and LAI_{init} are not applicable to evergreen phenology because plants are always in the "normal growth" state [*Ivanov et al.*, 2008a]. The parameter f_{LS} is the fraction of living sapwood in sapwood biomass [*Friend et al.*, 1997] that is used to ensure that a sufficient woody and root biomass is present to support leaves: $f_{LS}(C_{sapw} + C_{root}) \geq \varepsilon_s\, C_{leaf}^{\epsilon}$ (a modified equation (73) in the work by *Ivanov et al.* [2008a].) The parameter D_0 [*Pa*] is the coefficient of stomatal sensitivity to humidity deficit [*Leuning*, 1995].

water can leave the domain through the saturated part of the boundary. For all other sides of the hillslope, the no-flux boundary condition was specified.

[8] Generic evergreen shrubs were imposed as the only vegetation type. Each computational cell was assumed to be occupied by a shrub with its state characteristics uniformly distributed in the horizontal plane. Canopy and sapwood biomass pools were dynamically simulated. The vertical distribution of roots, quantifying the relative strength of soil moisture uptake, were assigned based on data available from previous studies [*Cox et al.*, 1986] for the Lucky Hills research site. The maximum depth of fine roots was assigned to 0.79 m, as the extrapolated depth of zero root biomass (the lowest depth with observed non-zero biomass is at 0.73 m). The utilized root profile has a typical power law decay shape [e.g., *Jackson et al.*, 1996] with maximum of root density occurring at 0.1 m. The profile was considered to be time-invariant in simulations and therefore in steady state with the imposed climate and distribution of nutrients in soil (not considered by the model). An implicit assumption then is that the long-term dynamics should be well captured by the model, given a non-transient climate forcing. The effects of profile time-invariance on simulation results in any given year are uncertain. To authors' knowledge, there is no firm evidence that root re-adjustment can be rapid and respond to deviations in seasonal distribution of rainfall. A priori, a certain lag in the root dynamics might be introduced by the long-term mean distribution of the nutrient pool.

[9] The shrub type has been parameterized using values partly reported by *Ivanov et al.* [2008a] and values obtained in the model confirmation study [*Ivanov et al.*, 2008c]. Table 1 reports the parameter values used in this study. Note that similar to *Gutiérrez-Jurado et al.* [2006], a continuous function has been used for constraining photosynthesis/root water uptake depending on soil moisture availability: $\beta_{T,i}(z_i) = a_T \exp(\psi_i(z_i))$, where $\beta_{T,i}$ is the factor associated with the layer i located at depth z_i [see *Ivanov et al.*, 2008a, equation (B12)], ψ_i is the negative soil matric pressure in *MPa* at that depth, and $a_T = 0.307$ is the fit parameter obtained from the data presented by *Pockman and Sperry* [2000] for creosote bush. This approach permits limited transpiration for very dry soil conditions (highly negative soil water pressures ψ). This is consistent with measurements of latent heat at the Lucky Hills site and an observed decline in water uptake with decreasing moisture in desert species, such as creosote bush [*Pockman and Sperry*, 2000]. Note that the scheme explicitly accounts for both root and soil water distributions. The outcome of this superposition of the "sink" (roots) and availability ("soil water") functions has been demonstrated to be a non-unique behavior of transpiration flux with respect to the mean root moisture content [*Guswa*, 2005].

[10] In the base case scenario discussed first in the following, the climate type was selected based on the criterion of its representativeness for the area surrounding the Biosphere 2 facility. The corresponding semiarid precipitation and radiation regimes lead to the most active phase (highest rates of productivity) of the growing season driven primarily by summer monsoons, when $\simeq$50% of the annual precipitation falls. Observational data for the Lucky Hills site [see *Scott et al.*, 2000; *Keefer et al.*, 2008], 31.73°N 110.05°W, 1370 m.s.l., were used as hydrometeorological forcing, spanning the period between 07/12/1996 and 01/20/2008. The 2 or 3.4 m level (depending on the measurement) data exhibit the following mean annual characteristics: precipitation is 349 mm, density of shortwave radiation flux on a horizontal plane is 245 W m^{-2}, air temperature is 17.2°C, atmospheric water vapor pressure is 805 Pa, and wind speed is 2.79 m s^{-1}. While environmental conditions inside the Biosphere 2 facility will be different from those corresponding to the Lucky Hills site, it is beyond the scope of this study to address these design concerns.

[11] The initial conditions need to be specified for both soil moisture and vegetation states. The initial soil moisture was obtained as the median value in mid-July for a simulation carried out for a level plot-scale site using the entire duration of meteorological series. It was assigned to be a uniform value of 0.143 [m^3 m^{-3}] with depth at each location of the domain as, a priori, it is expected to have an insignificant effect on the long-term dynamics. Initial densities of biomass pools corresponding to the compartments of canopy, live sapwood, and fine roots were obtained as the mean values obtained in the same simulation for the time period corresponding to mid-July: canopy - 40 [g C m^{-2}], live sapwood (parenchyma cells) - 80 [g C m^{-2}], and live fine

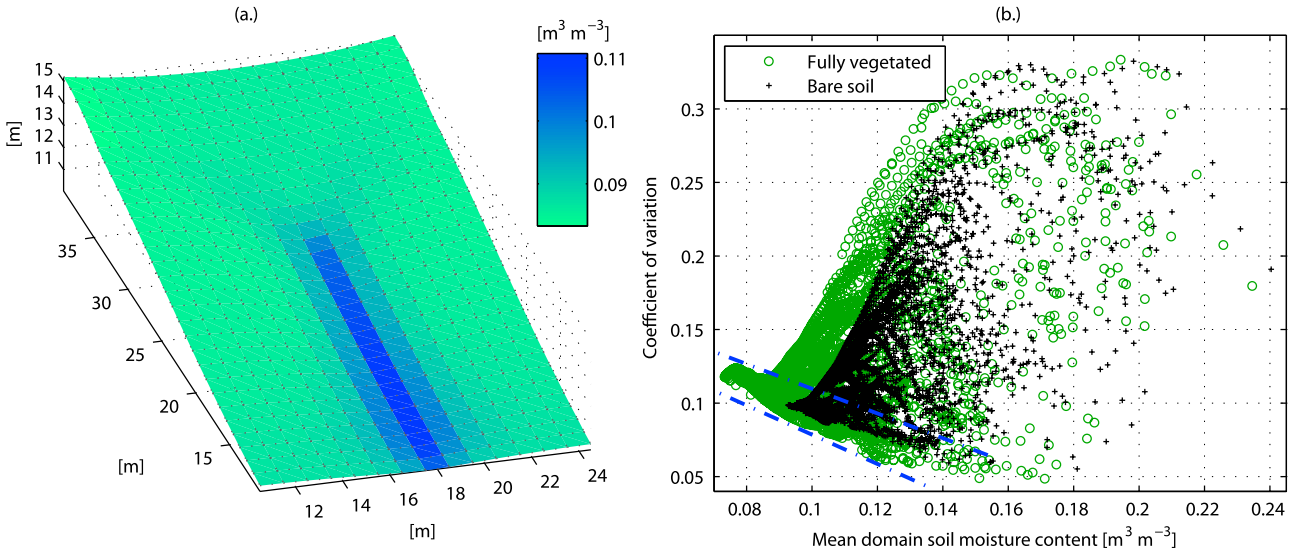

Figure 1. The results of continuous 11-year long simulations illustrating (a) the spatial distribution of mean root soil moisture and (b) the coefficient of variation of depth-integrated soil moisture content as a function of its mean daily value over the Biosphere 2 domain. The results correspond to fully vegetated (Figures 1a and 1b) and bare soil (Figure 1b) scenarios.

root - 75 [g C m^{-2}]. The long-term stationarity of the selected biomass densities for the imposed stationary climate, i.e., a consistent time-evolution around the long-term mean, was verified in spin-up experiments. Additionally, it has been confirmed that using either spatially uniform or spatially distributed (assigned as the long-term means for each individual location) biomass pools in the initialization did not lead to any appreciable differences in the simulations results. This is presumably because of the domain mild topography that leads to ~19% average difference between maximum and minimum long-term mean biomass densities in the domain and the chosen plant type that adjusts to the climate- and topography-dictated spatial distribution over the period of 2–3 years. The main conclusions of this study are therefore insensitive to these two possible types of vegetation initialization.

[12] Two long-term simulation scenarios will be presented, corresponding to the fully vegetated and bare soil cases. These two scenarios are constructed to investigate the differences that dynamically evolving plants introduce into the domain soil water dynamics. Such differences are the result of changes in the intertwined physical processes that vegetation directly impacts by intercepting rainfall, taking up moisture from the root zone, modifying surface long- and shortwave energy budgets, and affecting surface roughness and stability of atmospheric boundary layer. All of these processes, for the vegetated surface, depend on the canopy state and the time evolution of the associated effects is therefore complex. An analysis developed in the following integrates results for the two cases over long-term scales.

3. Analysis of Soil Moisture Spatial Variability

3.1. Long-Term Vegetation-Hydrology Dynamics and the Existence of State "Attractor" Space

[13] In the base case scenario, the Biosphere 2 domain was forced with the 11-year hydrometeorological series measured at the Lucky Hills site. Rainfall was assumed to fall vertically [*Ivanov et al.*, 2008b]. Vegetation dynamically evolved in time, responding and feeding back to the simulated above and below-ground conditions. In a similarly designed experiment, vegetation was entirely removed and heat and moisture regimes were simulated for bare soil only. The results of these experiments are shown in Figures 1a and 1b. As can be seen in Figure 1a, while the domain has relatively mild topographic features and the soil is isotropic, the combination of these conditions with high soil conductivity as well as the existence of a shallow impervious soil bottom boundary resulted in appreciable spatial inhomogeneities. The differences in the long-term mean soil moisture content in the root zone can be clearly discerned in Figure 1. The results are consistent with qualitative expectations of general behavior: the trough in the middle of the domain exhibits higher temporal variability of soil water (not shown) and mean moisture content, despite active uptake by vegetation. This leads to a somewhat higher productivity (by ~15–20% with respect to the rest of the domain) and average standing biomass in this area of topographic convergence. Relatively higher variability of the mean root moisture can be observed in the downslope fraction, apparently attributed to the more divergent features of the topography in that area.

[14] Figure 1b illustrates the coefficient of spatial variation C_v of the total moisture content θ simulated at each mesh location (i.e., moisture integrated over the entire depth of the soil profile) plotted versus its spatially mean value, $\overline{\theta}$. The illustrated simulation results have been averaged to the daily scale from the hourly instantaneous values. Two scenarios are shown corresponding to the fully vegetated and bare soil cases.

[15] Note that due to current observational limitations in the subsurface, most empirical studies can only focus on spatial variability of shallow surface moisture [e.g., *Famiglietti et al.*, 1999; *Choi and Jacobs*, 2007; *Famiglietti et al.*, 2008]. Such studies are useful for understanding statistical variability due to, presumably, dominant local

factors (such as inhomogeneities of soil texture/structure and soil radiation balance because of the differences in the canopy cover, etc.) but have a limitation of resolving nonlocal controls, such as subsurface flows that are not necessarily shallow.

[16] While also feasible in this modeling study, choosing surface soil moisture as the metric of interest would inhibit insights into the mechanisms that may truly dominate in the hydrologic response. One example is that for coarse soils, conditions at shallow depths could be essentially de-coupled from deeper states of the soil. Generally, the dynamics of the saturated zone or the conditions of availability and uptake of moisture by plants cannot be reliably inferred from the spatial distribution of surface soil moisture only. The selected metric of depth-integrated moisture content therefore appears to be most appropriate for the analysis of spatial variability as it fully defines the state of the system between boundaries with specified conditions. Theoretically, this is a consistent metric that should provide insights into the interplay of mechanisms leading to particular dynamics of $\overline{\theta}$.

[17] Figure 1b shows several interesting features including the high density band of simulated data points at the bottom of the $C_v(\overline{\theta})$ patterns (outlined with the dash-dot lines), the overall non-unique behavior of the $C_v(\overline{\theta})$ relationship, and the relative differences of the $C_v(\overline{\theta})$ relationship between the vegetated and bare soil cases. The mechanistic interpretation of the band and its relation to the $C_v(\overline{\theta})$ pattern will be discussed first in the following for the fully vegetated case.

[18] Visually, the band of data points at the bottom of the $C_v(\overline{\theta})$ pattern corresponds to the lowest spatial variability of soil water content given $\overline{\theta}$. The band of $C_v(\overline{\theta})$ grows as the domain becomes drier because the standard deviation remains relatively constant and $\overline{\theta}$ decreases. The band should represent a physically identifiable part of the "phase space" of the hydrological system at this scale under stationary climate. It is hypothesized that the band characterizes the principal "*attractor*" of the domain states. Note the definition of the above terminology. The phase space is defined here as a representation of all possible changes that the dynamical (in this case hydrological) system could undergo over time [e.g., *Jayawardena and Lai*, 1994]; any point in the space corresponds to a possible state of the system. When the trajectories of system evolution follow a readily discernable pattern in the phase space, such a pattern is termed an "attractor". The phase space under consideration is represented by the two dimensions associated with two macroscopic quantities: mean domain soil moisture $\overline{\theta}$ and the coefficient of variation of depth-integrated soil moisture $C_v(\overline{\theta})$.

[19] Being an inherently dissipative entity, the hydrological system either (1) evolves along the attractor, when its initial state falls within/near it and any subsequent perturbations are small, or (2) evolves toward it, in the limit of the time dimension, when the initial state is off of the attractor phase space and/or subsequent perturbations are large. As pointed out in (1), the existence of such an attractor can be associated with a threshold effect, when a sufficiently large perturbation, i.e., a rainfall event, may initially deviate the evolution of the system away from the attractor space. As will be demonstrated in the following, this explains the existence of data points with higher C_v for any given $\overline{\theta}$. Thus hysteresis, broadly defined here as "memory" [e.g., *Krasnosel'skii and Pokrovskii*, 1989], of the $C_v(\overline{\theta})$ temporal evolution occurs. Finally, under stationary climate, one may also identify the limiting state as the driest conditions possible, which can be found on the left-hand side of the diagram in Figure 1b.

[20] Specific domain conditions and physical mechanisms lead to the existence of the hypothesized attractor. Topography, soil and bedrock types, their depth, permeability and homogeneity are the primary physical constraints. Precipitation is an essential factor determining perturbation magnitude. Evapotranspiration, predominantly mediated by existing vegetation, and subsurface flows are the mechanisms that evolve hydrological system to a particular state of its phase space. The role of subsurface flows could be of paramount importance in areas of complex topography, where spatial redistribution of moisture can be efficiently driven by gravity-induced gradients. Further, the hypothesis proposed here argues that the occurrence of conditions triggering or suppressing near-saturated subsurface lateral exchange is the essential reason leading to the observed $C_v(\overline{\theta})$ pattern. Within the context of information displayed in Figure 1b, if the domain state (characterized by the mean and spatial variance of soil moisture content) falls within the attractor space, then there is a likelihood that any following rainfall will not lead to topographic soil moisture redistribution and dynamics that could lead to the enhancement of heterogeneity will be suppressed. This implies that only larger precipitation events, exceeding a particular magnitude, could lead to evolution of soil moisture states that would fall outside of the attractor space in Figure 1b. Conversely, if the domain state has a combination of C_v and $\overline{\theta}$ that does not fall within the attractor band, topographic soil water redistribution is likely to be ongoing, either enhancing or diminishing with time, and will continue taking place with any subsequent wetting event. Thus, pre-event hydrological state of the domain, repeatedly characterized here as a combined metric of soil moisture spatial mean and variability, is argued to be one of the primary variables controlling the hydrological response in zero-order catchments. Hysteresis of the temporal evolution of metrics characterizing soil moisture spatial distribution as a function of mean state is an inherent property of such a system.

[21] Furthermore, system energy input translated into the strength of evaporative flux in non-limiting conditions can also be thought of as an important component affecting the occurrence of subsurface flows during interstorm periods. As the wetting front propagates through soil, local sinks may deplete moisture and suppress its efficient lateral redistribution. However, as will be shown later, for the considered soil type and magnitude of root moisture uptake, the role of evapotranspiration is fairly insignificant at short post-event scales but rather pronounced at longer timescales. Its primary effect is argued to be related to the rate of perturbation dissipation in the hydrological system, after an initial period of subsurface moisture redistribution. Ultimately, evapotranspiration determines the rate at which the system returns to or evolves within the attractor space.

3.2. Physical Mechanisms Leading to Hysteretic Pattern of $C_v(\overline{\theta})$

[22] The statements of section 3.1 a) referred to the hysteretic nature of the $C_v(\overline{\theta})$ pattern in the analyzed hydrological system; b) hypothesized the existence of the system

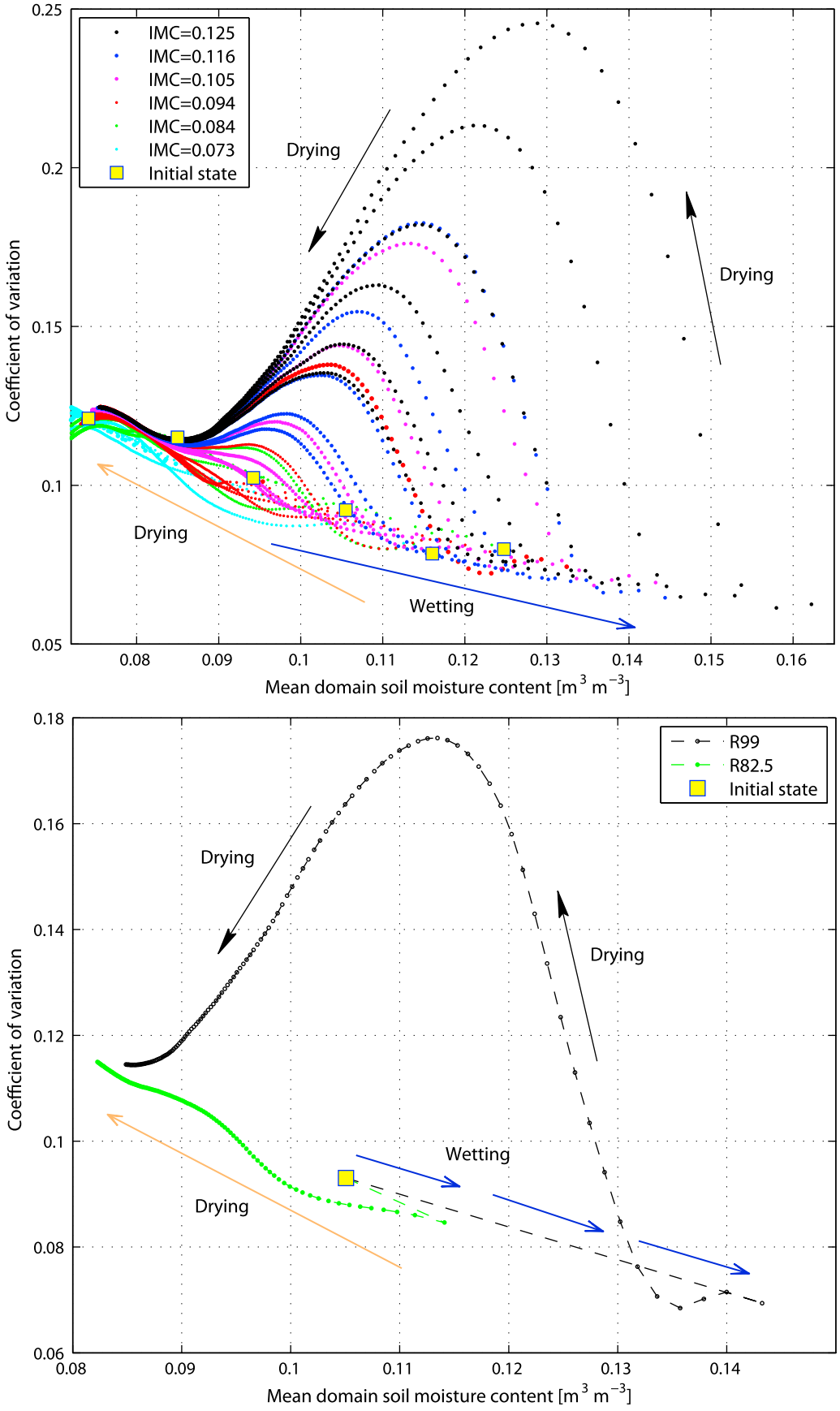
IMC=0.125
IMC=0.116
IMC=0.105
IMC=0.094
IMC=0.084
IMC=0.073
Initial state
Drying
Drying
Drying
Wetting
Coefficient of variation
Mean domain soil moisture content [m 3 m −3]
R99
R82.5
Initial state
Drying
Drying
Wetting
Drying
Coefficient of variation
Mean domain soil moisture content [m 3 m −3]

Figure 2

state "attractor" and conditions under which the system state evolves within or toward it, and c) pointed to the possible physical mechanisms responsible for such features. In order to support these statements/hypotheses, a set of synthetic experiments was designed. In all of these experiments, a single wetting event is followed by a long dry-down period.

3.2.1. Supporting Synthetic Experiments

[23] Six initialization states falling within the attractor space of Figure 1b were selected from the 11-year continuous simulation, with the mean volumetric moisture contents $\overline{\theta}_{ini}$ of the domain equal to 0.0742, 0.0843, 0.0936, 0.105, 0.116, and 0.125 [m^3 m^{-3}] and the corresponding coefficients of variation equal to 0.121, 0.118, 0.105, 0.0939, 0.0796, and 0.0811. In order to avoid significant transient effects in the soil water dynamics, it was ensured that in each of the cases interstorm conditions lasted for at least four days prior to the time of selected moisture distribution. For the cases of $\overline{\theta} \leq 0.0936$, the length of antecedent interstorms exceeded twelve days. The corresponding three-dimensional distributions of soil water content were used to explicitly initialize the pressure head distributions within the Biosphere 2 domain. Note that selecting initial states from those within the attractor space guarantees smallest possible C_v for a given $\overline{\theta}$ at the simulation start. As argued previously, different rainfall magnitudes can lead to different patterns of temporal evolution of $C_v(\overline{\theta})$ during the post-storm period. Therefore the chosen design allows the search of the perturbation magnitude required to deviate the evolution of the hydrological system away from the attractor. Stated differently, one can find rainfall for a given $\overline{\theta}$ required to trigger the subsurface exchange, thereby significantly increasing moisture spatial heterogeneity.

[24] In terms of hydrometeorological conditions, the month of August was chosen as the representative period during which most of the vegetation-hydrology dynamics occur in the area of interest, driven by monsoonal precipitation and abundance of light. A set of rainfall scenarios were applied to each of the generated initialization states. In these scenarios, precipitation totals, P_T, were equal to 6.2, 11.8, 17.7, 23.7, 32.1, and 41.5 mm that corresponded to 75, 82.5, 90, 95, 98, and 99th percentiles, n_P, of August daily rainfall (computed for rainy days only), as estimated from observational data for the Lucky Hills site. For each rainfall scenario, precipitation was specified to occur at the beginning of simulation and was distributed in two and a half hours, which approximately corresponded to the mean event duration for the month of August. This also ensured that none of the synthetic events lead to infiltration excess runoff since the imposed saturated hydraulic conductivity was 146 [mm hr^{-1}] (see section 2 above).

[25] Most of the other hydrometeorological variables required for simulations, i.e., atmospheric pressure, air humidity, temperature, and wind speed were specified as their mean daily cycles for the month of August and used as forcing in each day of the considered simulation period. Input of shortwave radiation was assigned using a weather generator (S. Fatichi et al., Simulation of future climate scenarios with a weather generator, submitted to *Advances in Water Resources*, 2009) as a daily cycle corresponding to the 90th percentile of the total daily energy input for the month of August (326 W m^{-2}). All simulations were carried out for a 12-month period. The domain became very dry at the end of each simulation, which ensured that each scenario included the period of primary interest (see below). The same vegetation initialization as in the base case scenario was assumed in each of the scenarios. Additional analysis indicated that essential inferences of this study are completely insensitive with regards to whether uniform (long-term average over the entire domain) or spatially-varying (long-term average at each location) plant biomass pools are used. Obviously, vegetation gradually dies during each of these simulations because of growing lack of soil moisture. Nonetheless, the period of primary interest for the following analysis spans 1.5–2 months since the simulation start, during which biomass changes are insignificant.

3.2.2. Analysis of Results

[26] The dark "Wetting" arrow in Figure 2 (top) indicates the principal direction of domain state evolution during a precipitation or, equivalently, a "perturbation" event. After the occurrence of an event, if the perturbation is small, spatial variability of soil moisture will not change significantly, staying within the band of the attractor space. The latter is reproduced in these experiments by aggregation of dots at the bottom of the pattern shown in Figure 2 (top). The overall, fairly linear time-evolution path of the state is indicated by the lightly colored "Drying" arrow pointing to the left. As argued previously and will be explicitly illustrated in the following, in this situation the subsurface lateral exchange is insignificant and rapidly suppressed by evapotranspiration. As event water percolates through the soil layer, it is taken up by roots; little reaches the soil bottom to produce the saturated conditions. Local processes (soil evaporation and transpiration) dominate the soil water dynamics. The temporal change in the spatial variability of depth-integrated soil moisture is then caused only by differences in the incoming shortwave energy and local vegetation state. Both of the latter depend on topography either explicitly (i.e., surface irradiance) or implicitly (i.e., plants). Therefore the slope of the attractor space band should also be a function of topographic conditions in the domain.

[27] Conversely, if the perturbation is sufficiently large, the evolution of domain state in time t leads to a pattern of $C_v(\overline{\theta}(t))$ that deviates from the attractor band, exhibiting a negatively skewed shape (Figure 2, top). The corresponding temporal dynamics of the soil moisture standard deviation exhibit the same patterns (not shown). The overall time-evolution path after the rainfall has ceased is indicated by the dark "Drying" arrows drawn in the immediate vicinity

Figure 2. The results of the dry-down experiments illustrating (top) thirty six 12-month long simulations that start from different initializations (Initial Moisture Contents, "IMC") and (bottom) two 4-month long simulations that have the same initial state (IMC = 0.105). In the case of Figure 2 (top), six initializations are forced with six precipitation totals corresponding to n_P = 75, 82.5, 90, 95, 98, and 99th percentiles of daily rainfall. In the case of Figure 2 (bottom), precipitation totals corresponding to either n_P = 99 ("R99") or n_P = 82.5 ("R82.5") percentiles are used. The square symbols denote the domain initial states and dots characterize the soil moisture mean and spatial variability on any given day. The dots of the same color and size indicate a simulation case with the same initialization.

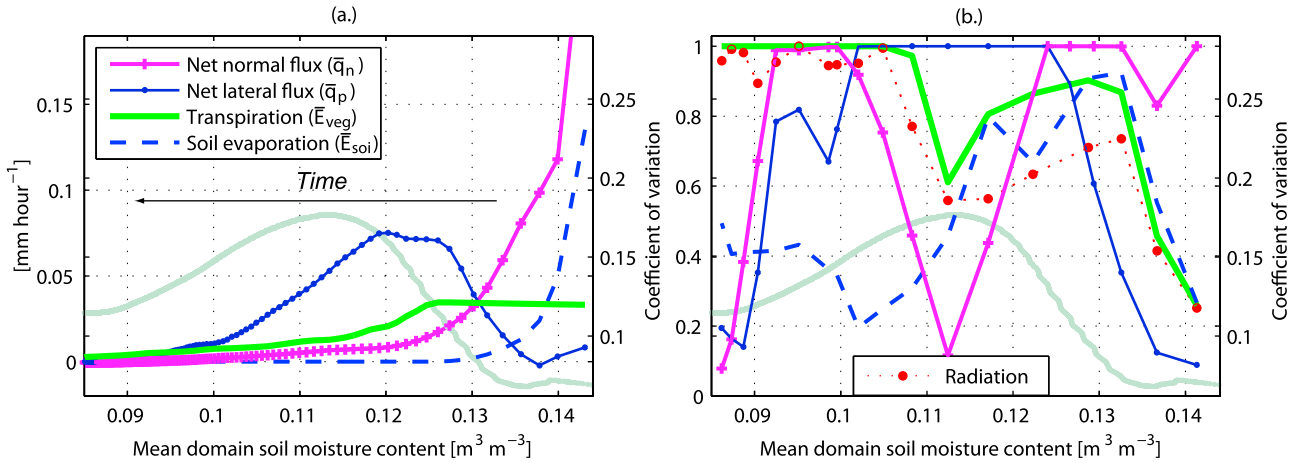

Figure 3. The presented results correspond to a dry-down scenario following a wetting event. The case of Figure 2 (bottom) for the rainfall of n_P = 99th percentile is illustrated: (a) spatially-averaged fluxes $\overline{q}_n$, $\overline{q}_p$, $\overline{E}_{veg}$, and $\overline{E}_{soi}$ and the coefficient of variation $C_v(\overline{\theta})$ plotted as functions of the mean domain moisture content $\overline{\theta}$ and (b) the posterior probabilities quantifying the importance of including a specific covariate $\overline{q}_n$, $\overline{q}_p$, $\overline{E}_{veg}$, $\overline{E}_{soi}$, or $\overline{S_{atm}}\downarrow$ as a linear regressor of spatial organization of depth-integrated soil moisture. The plotting styles in Figure 3b are those that are used for the corresponding covariates in Figure 3a. The light green line in the background is the series of $C_v(\overline{\theta})$ with the corresponding y axis on the right hand side of both of the plots. The temporal evolution can be envisioned by tracking all series from the right to the left side of the plots.

of the data points corresponding to the simulation scenario with $\overline{\theta}_{ini}$ = 0.125 and n_P = 99. In such cases, the hydrological response of the system can be attributed to rapid percolation of event moisture down to the impervious bottom of the soil profile, passing beyond depth where access by roots is possible, and generation of saturated (or nearly-saturated) conditions that result in efficient subsurface exchange. Return flow through the seepage face is produced. For the considered domain, lateral exchange is always possible as the bedrock topography replicates domain surface terrain and thus gravity-induced gradients of the pressure head act to redistribute moisture, provided the flow medium is sufficiently conductive. Non-local dynamics thus begin to dominate in determining soil water spatial variability. The period over which the first maximum in $C_v(\overline{\theta}(t))$ is attained can be considered as the "effective period of redistribution." While the interplay among the various processes is complex and changes with time, over this time interval, topography-induced lateral exchange of moisture is one of the dominant processes contributing to the spatial variability of soil moisture (a more detailed analysis is presented below). As can be inferred from Figure 2 (top), this period generally varies with both the initialization state and rainfall magnitude. For instance, for initialization $\overline{\theta}_{ini}$ = 0.125, the period duration is between 15 days (n_P = 99) and 28 (n_P = 75) days. It might be generally noticed that the duration of the effective redistribution period increases with lower rainfall magnitude for the same initialization state. This is likely due to a decrease in effective conductivity of the soil media that positively correlates with the amount of moisture coming from the imposed precipitation. Evapotranspiration acts to slow down the percolation process, especially when its rate is comparable to the rate of water flux in the soil, further delaying accumulation of moisture above the bedrock face. Once domain spatial variability is maximized, expressed as the peak in $C_v(\overline{\theta}(t))$, the strength of evapotranspiration sink defines the rate at which the topography-induced heterogeneity is destroyed. The hydrological system returns to the attractor space, which is illustrated by the descending limbs of the $C_v(\overline{\theta}(t))$ curves in Figure 2 (top).

[28] Overall, as seen in Figure 2 (top), the non-uniqueness of the $C_v(\overline{\theta}(t))$ relationship is easily reproduced in these simplified experiments that contain a single rainfall event at the beginning, with a subsequent long dry-down period. Except for the cases with $\overline{\theta}_{ini}$ = 0.0742, 0.0843, in which any imposed rainfall is not sufficient to trigger subsurface moisture exchange, the time-evolution patterns are consistent with the hypotheses set forth previously, i.e., there exists a system attractor space and temporal change of soil moisture variability depends on both the system initial state and rainfall magnitude, exhibiting hysteresis. The key difference between the above experiments and the long-term continuous simulation (discussed in 3.1) is that in the latter case the state of the domain may frequently not reach the attractor space before a subsequent precipitation event breaks the interstorm period. This further complicates the hysteretic nature of the $C_v(\overline{\theta}(t))$ relationship and results in numerous values of coefficient of variation for the same value of $\overline{\theta}$.

[29] To obtain deeper insights on the interplay of physical mechanisms leading to the observed behavior, a subset of simulation results used in Figure 2 (top) is shown in Figure 2 (bottom), corresponding to a single initialization $\overline{\theta}_{ini}$ = 0.105 with n_P = 82.5 (P_T = 11.8 mm) and n_P = 99 (P_T = 41.5 mm). As seen in Figure 2 (bottom), the overall time-evolution paths have been already described in the previous discussion, which pointed to the possibility of distinct differences in the domain response. Both rainfall events lead to initially higher mean moisture and lower spatial variability, denoted by the first dot to the right of both of the initialization states. In the case of n_P = 82.5, the spatial variability in the hydrological system evolves within the attractor space; in the case of n_P = 99, heterogeneity of soil moisture strongly increases initially

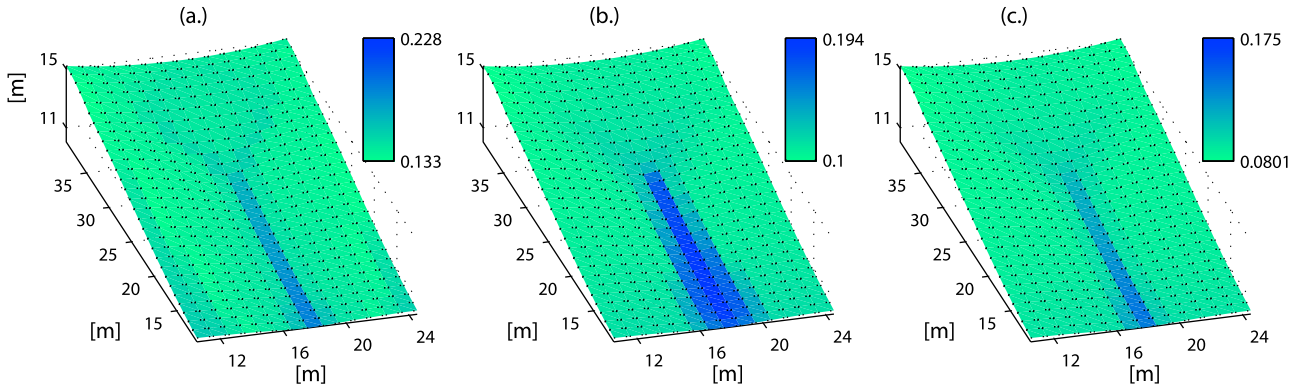

Figure 4. Instantaneous spatial distributions of depth-integrated soil moisture for a dry-down scenario following a wetting event. The scenario corresponds to the case of Figure 2 (bottom) for rainfall of n_P = 99th percentile: (a) hour 24: $C_v(\overline{\theta})$ is at minimum and equals 0.068 with $\overline{\theta}$ = 0.136; (b) hour 546: $C_v(\overline{\theta})$ is at maximum and equals 0.176 with $\overline{\theta}$ = 0.113; and (c) hour 1884: a late stage of decrease in $C_v(\overline{\theta})$, which equals 0.119 with $\overline{\theta}$ = 0.09.

and gradually dissipates after the effective redistribution period has been reached. Note that in the latter case, during the first three days after the rainfall event, spatial variability remains fairly constant or even has a tendency to decrease. Theoretically, this period should correspond to the effective period of vertical flow of soil water during which saturation builds up at the bottom of the soil profile, creating gradients sufficient for subsequent lateral exchange. Further supporting analysis of this statement will be presented in the discussion that follows.

[30] Physical but insofar qualitative interpretations of the presented results have been attempted, however, further quantitative evidence is warranted. The main purpose of the analysis would be to attribute the various stages of the $C_v(\overline{\theta}(t))$ dynamics to dominant processes that change as the hydrological response evolves in time. Figures 3 and 4 analyze the scenario illustrated in Figure 2 (bottom) for the rainfall case of n_P = 99.

[31] Since after the first day (omitted in the following analysis) the mean moisture continuously decreases in time, the temporal evolution of the system can be tracked from the right side of the plots to the left. The domain-averaged mean daily rates of water fluxes scaled to a unit area of level surface are plotted in Figure 3a. They represent (1) the net moisture flux normal to terrain surface, $\overline{q}_n$, quantifying percolation rate as the depth-integrated normal component of the flow [*Ivanov et al.*, 2008b]; (2) the net lateral influx, $\overline{q}_p$, illustrating the intensity of lateral subsurface exchange as the depth-integrated difference between influxes and outfluxes in all domain interior nodes; (3) transpiration, $\overline{E}_{veg}$, as

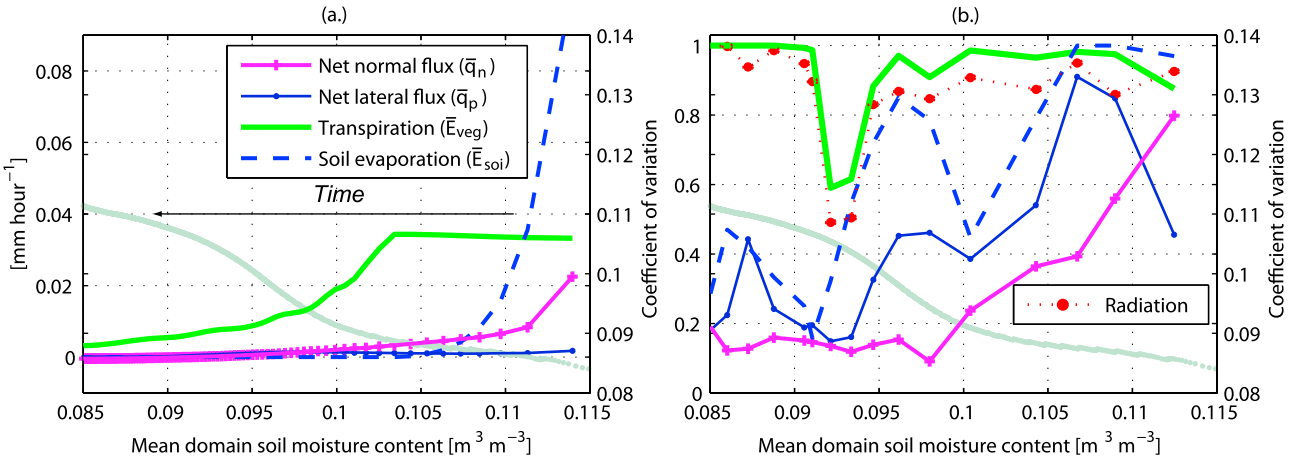

Figure 5. The presented results correspond to a dry-down scenario following a wetting event. The case of Figure 2 (bottom) for the rainfall of n_P = 82.5th percentile is illustrated: (a) spatially-averaged fluxes $\overline{q}_n$, $\overline{q}_p$, $\overline{E}_{veg}$, and $\overline{E}_{soi}$ and the coefficient of variation $C_v(\overline{\theta})$ plotted as functions of the mean domain moisture content $\overline{\theta}$ and (b) the posterior probabilities quantifying the importance of including a specific covariate $\overline{q}_n$, $\overline{q}_p$, $\overline{E}_{veg}$, $\overline{E}_{soi}$, or $\overline{S_{atm}}\downarrow$ as a linear regressor of spatial organization of depth-integrated soil moisture. The plotting styles in Figure 5b are those that are used for the corresponding covariates in Figure 5a. The light green line in the background is the series of $C_v(\overline{\theta})$ with the corresponding y axis on the right hand side of both of the plots. The temporal evolution can be envisioned by tracking all series from the right to the left side of the plots.

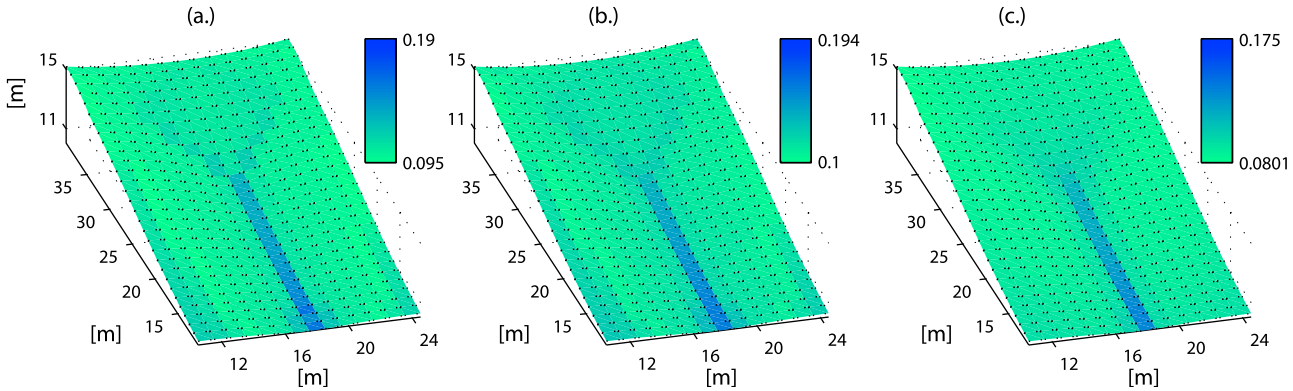

Figure 6. Instantaneous spatial distributions of depth-integrated soil moisture for a dry-down scenario following a wetting event. The scenario corresponds to the case of Figure 2 (bottom) for rainfall of n_P = 82.5th percentile: (a) hour 0: $\overline{\theta} = 0.105$, $C_v(\overline{\theta}) = 0.093$; (b) hour 42: $\overline{\theta} = 0.113$, $C_v(\overline{\theta}) = 0.085$; and (c) hour 188: $\overline{\theta} = 0.09$, $C_v(\overline{\theta}) = 0.108$.

the rate of moisture uptake by roots in the first 79 cm of soil; and (4) soil evaporation, $\overline{E}_{soi}$, which is applied as the moisture sink to the soil surface layer (first 20 mm). As time progresses, which can be envisioned by tracking the series from the right to the left side of the plot, the flux rates exhibit different dynamics. The flux $\overline{q}_n$ peaks at the beginning during the period of moisture vertical redistribution, when the wetting front is above the soil bottom. As the percolation flux reaches the bedrock surface and spatial gradients are generated, the lateral flow starts to increase, which is illustrated by the dynamics of $\overline{q}_p$. After some time, the flux $\overline{q}_p$ reaches the maximum value that is likely associated with maximum concentration of moisture near the domain trough area. When soil water reservoir is undepleted, both $\overline{E}_{veg}$ and $\overline{E}_{soi}$ are at maximum. The latter flux rapidly decays in time due to the depletion of surface soil moisture and weak soil capillarity. Vegetation uptake remains initially constant, as the applied meteorological forcing is replicated in each day, but starts to decrease once vegetation begins to experience moisture limitation and slowly dies. Apparently, as the domain gradually dries out, both due to flow through the seepage face and the evapotranspiration process, the mean fluxes diminish in their magnitudes. Figure 5a illustrates the same fluxes for the scenario shown in Figure 2 (bottom) but for the rainfall case of $n_P = 82.5$.

[32] In order to make a quantitative statement with regards to the transition of controls on the spatial variability of θ among these processes, spatial covariances of depth-integrated soil moisture θ with several flux variables are analyzed. A geostatistical regression approach [e.g., *Erickson et al.*, 2005] is used to represent the instantaneous values of local depth-averaged soil moisture θ as a linear combination of site-specific fluxes of q_n, q_p, E_{veg}, E_{soi}, and $S_{atm} \downarrow$ (incident shortwave radiation) at the hourly time step. The applicability of linear analysis is certainly questionable, especially for the periods with high $C_v(\overline{\theta})$. Nonetheless, the goal is not to fit a perfect statistical model but rather identify a temporal shift in the dominant model regressors, i.e., those that are likely to control the pattern of θ in space. More specifically, at each hour, $(2^5 - 1)$ linear combinations of regressors q_n, q_p, E_{veg}, E_{soi}, and $S_{atm} \downarrow$ are tested as predictors of θ (note that '5' is the total number of regressors). Obviously, these variables exhibit temporal dynamics of cross-correlation among themselves. This makes difficult the identification of importance of individual covariates (e.g., q_n, q_p, etc.) with more traditional statistical techniques, such as the Principal Component Analysis, which is not concerned with the individual contributions of regressors. The utilized technique is thus based on the Bayesian Information Criterion (BIC) [*Schwarz*, 1978]. The method assigns Bayes factors that compares several alternative models simultaneously. It is based on the notion that candidate models should be compared in terms of prior and posterior information that provides evidence for a model over an alternative model [*Raftery*, 1995; V. Yadav et al., A geostatistical synthesis study of factors affecting net ecosystem exchange in various ecosystems of North America, submitted to *Biogeosciences*, 2009]. The associated probabilities quantify the need to include a given covariate into the geostatistical linear regression model, i.e., the higher the probability, the higher the likelihood that the covariate contributes to the spatial variability of soil moisture at a given instant. As a "rule of thumb", probabilities higher than 0.9 indicate a robust statistical significance. The results of the BIC analysis are shown in Figures 3b and 5b. Snapshots of instantaneous θ spatial distribution at different times are illustrated in Figures 4 and 6. The output times were selected based on the temporal evolution of $C_v(\overline{\theta})$ in Figure 2 (bottom).

[33] It is expected that the system heat regime exhibits a diurnal cycle because of the cycle of the energy input, i.e., $S_{atm} \downarrow$. Because of the evapotranspiration process, the mass flow regime is coupled to the heat regime and therefore it is expected that all of the above regressors exhibit diurnal dynamics, which are reflected in the computed BIC probabilities. In order to eliminate these high-frequency effects, the probabilities were averaged over the 4-day time step.

[34] As Figure 3b shows, the increase of $C_v(\overline{\theta})$ (following the temporal evolution from the right side of the plot to the left) appears to be predominantly related to the normal redistribution flow, evapotranspiration, and lateral flow. The latter flux appears to be one of the most important variables throughout the period of the ascending limb of $C_v(\overline{\theta})$ because of the highest BIC probabilities for $\overline{\theta} > 0.127$. It is apparent, nonetheless, that the resulting temporal evolution of soil moisture spatial variability is an outcome of the

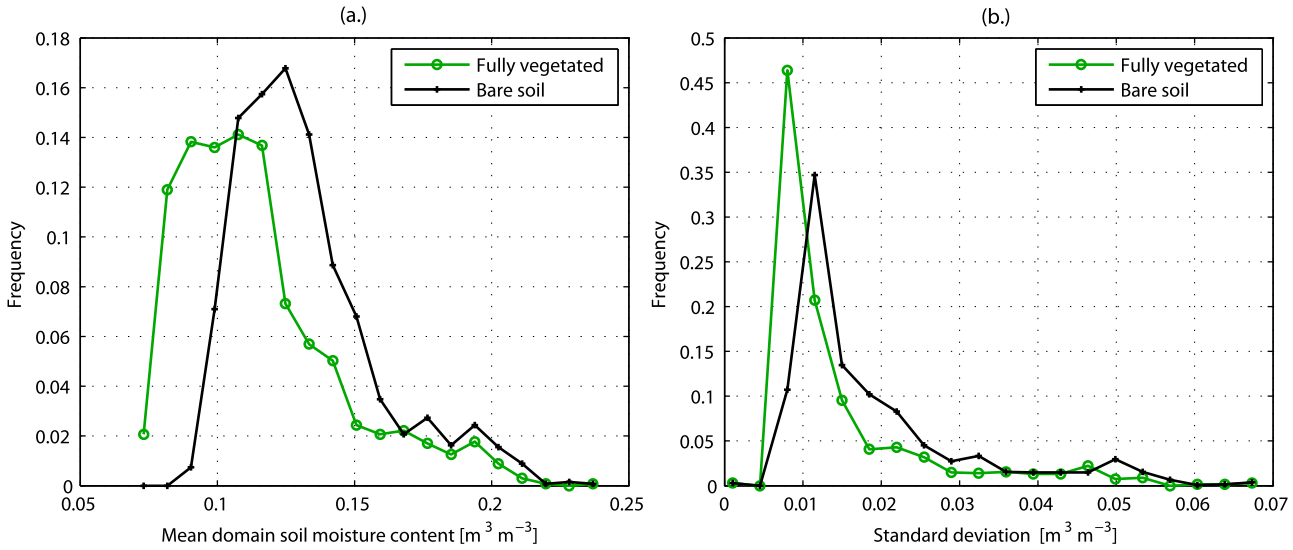

Figure 7. Frequency distributions of (a) mean domain soil moisture during the days immediately preceding storms and (b) mean standard deviation of soil moisture during interstorm periods. The distributions were inferred based on the results of 11-year long simulations.

interplay among all involved processes. As pointed out, all of them exhibit diurnal cycles (not illustrated), which likely implies diurnal shifts in controls of soil moisture spatial variability. Note also that the peak of $\overline{q}_p$ (Figure 5a) occurs before $C_v(\overline{\theta})$ reaches its highest value, although, a priori, one could hypothesize that the two maxima should be co-located in time. A possible (but hardly verifiable) argument is that when the net subsurface moisture exchange reaches the highest rate, other processes are at work to effectively decrease the corresponding effect on moisture spatial variability. Since the effect of these processes must be declining with time, the highest spatial variability of moisture occurs later, when the magnitude of net lateral exchange is lower but still non-negligible. The time point when $C_v(\overline{\theta})$ reaches its maximum ($\overline{\theta} \simeq 0.113$, Figure 4b) has been argued to imply the end of the effective redistribution period. At that time, the significance of q_n and E_{veg} fluxes in explaining the pattern of θ in space is at the minimum (Figure 3b) and q_p is the only variable that has non-negligible explanatory power according to the BIC analysis.

[35] After the peak of $C_v(\overline{\theta})$ has been reached, plant moisture uptake gradually homogenizes soil moisture. A temporary increase of the significance of q_n at $\overline{\theta} \simeq 0.1$ (Figure 3b) is likely associated with the capillary pull of water from the wetter layers below the root zone. The effect is of short duration, presumably because of the weak soil capillarity that cannot sustain vertical flux when an appreciable distance forms between the bottom of the root zone and an underlying wet layer. Subsurface moisture exchange still occurs but its importance is decreasing in time, becoming negligible at later stages of the simulation period (Figure 4c).

[36] Note the difference in the y axis scales in Figures 3a and 5a. Figure 5b demonstrates the relative insignificance of q_n and q_p throughout the entire simulation period for the scenario corresponding to the case of system evolution within the attractor space (the rainfall case of $n_P = 82.5$). As Figures 6b and 6c illustrate, the spatial distribution of soil moisture does not substantially change from the initialization distribution (Figure 6a), in relative terms. This is not the case for the distributions shown in Figures 4b and 4c, corresponding to the same values of $\overline{\theta}$. Overall, transpiration (correlated with energy input) dominates throughout the entire period thus confirming the predominant control of local dynamics in determining soil moisture spatial variability. Note that as discussed in the beginning of section 3.2.2, the temporal change in the spatial variability is caused only by differences in the incoming shortwave energy and local vegetation state. Both depend on topography but are fairly insignificant.

4. Long-Term "Homogenizing" Effect of Vegetation

[37] The preceding analysis has argued that pre-event state of the domain, characterized as a combined metric of both soil moisture spatial *mean* and *variability*, and rainfall magnitude are the primary variables controlling post-event dynamics in relation to the attractor space. In this context, the long-term characteristics of pre-event states deserve a special discussion as they determine a general pattern of partitioning of the post-event system water budget.

[38] Evapotranspiration is usually one of the most significant terms in the soil water balance of systems located in semiarid regions [e.g., *Noy-Meir*, 1973]. Plant moisture uptake typically dominates over soil evaporation [e.g., *Guswa et al.*, 2002]. The results of the long-term simulations, partially illustrated in Figure 1b, agree with this statement: in the fully vegetated case, ~64% of incoming precipitation leaves the domain due to evapotranspiration process, whereas only ~36% is evaporated in the bare soil case. When integrated over the long-term period, root moisture uptake leads to generally drier pre-event states and more homogeneous post-event spatial distributions in the vegetated case, as compared to the bare soil case (Figures 7a and 7b). The median value of the pre-storm mean domain soil moisture $\overline{\theta}_{ini}$ is 0.108 and the median value of the standard deviation of soil moisture during all interstorm

periods is 0.0098; in the bare soil case, these values are 0.126 and 0.0138, correspondingly.

[39] These values indicate that pre-storm states of the vegetated case are likely to be near the identified attractor space, while they are more likely to be off the attractor band in the bare soil case. Vegetation function therefore results in pre-storm states that, overall, increase the likelihood that a rainfall event will not lead to efficient lateral subsurface exchange, i.e., the post-wetting topographic redistribution of soil water is suppressed by local processes of transpiration and soil evaporation. Using a surrogate metric to quantify soil water redistribution efficiency: the total computed flux through the downslope seepage boundary for the vegetated case is only 57% of that for the bare soil case. The state of the vegetated domain thus has the tendency to stay within the attractor space characterized by smaller spatial heterogeneity relative to the case when re-distribution occurs. The results indicate that the state of the vegetated domain is within the attractor space approximately ~57% of the simulation period, while the latter number is ~21% for the domain with bare soil conditions. Consequently, vegetation function appears to exert a relatively "homogenizing" effect on domain soil moisture over the long-term scales.

[40] Note that the term "homogenization" is essentially applied in a comparative sense. It refers to the theoretically higher likelihood of evolution of domain state within the attractor space during interstorm periods and higher perturbations that are required to deviate the evolution of the system away from the attractor space. While both of these conditions are applicable to the vegetated case, most of the mass of its attractor space can be attributed to the drier part of the analyzed pattern. As can be seen in Figure 1b, $C_v(\overline{\theta})$, in fact, grows within the attractor space as the domain becomes drier because the standard deviation remains relatively constant and $\overline{\theta}$ decreases. In the bare soil case, redistribution occurs more frequently. The corresponding coefficients of variation, however, do not significantly exceed the values of $C_v(\overline{\theta})$ for the vegetated case, most of which are associated with the drier part of the attractor band (to the left of the symbols for the bare soil case in Figure 1b), where $C_v(\overline{\theta})$ is higher. The outcome is that the probability density functions of $C_v(\overline{\theta})$ do not differ significantly between the bare soil and vegetated cases, although the underlying mechanisms for that are different. "Homogenization" implied here nonetheless does entail a lower absolute variability of soil moisture during interstorm periods (Figure 7b).

5. Discussion

[41] Hillslopes or, almost equivalently, zero-order catchments, are fundamental structural units of the landscape [*McDonnell*, 2003; *Troch et al.*, 2003; *Tromp-van Meerveld and Weiler*, 2008]. The spatiotemporal superposition of their responses to a hydrometeorological event underlies the hydrological response characteristics of basins of higher orders. Therefore, it is of primary importance to understand the physical mechanisms that underlie heterogeneity of states and fluxes in these simple-geometry topographic units [*Weiler and McDonnell*, 2004; *Tromp-van Meerveld and Weiler*, 2008]. This study addresses such effects and makes inferences about relevant mechanisms.

[42] The study has argued for the existence of the attractor space for domain soil moisture state and demonstrated the conditions at which the system hydrological response can evolve within or toward it. As an intrinsic feature of these conditions, the study also identified and illustrated hysteresis of spatial variability of depth-integrated soil moisture. The effect of hysteresis had been previously noted in data and simulations for different integration depths. For example, the quasi-spatial model of *Teuling and Troch* [2005] produced the effect (top 20–30 cm) but no exact mechanistic explanation was offered; later, *Teuling et al.* [2007] identified the characteristic effects of climate variability on the hysteresis of root zone soil moisture (top 20 cm). At the basin scale, *Vivoni et al.* [2010] argued for the transition of controls in the hysteresis of surface (top 10 cm) soil moisture spatial variability from precipitation (wetting stage) to landscape (drying stage) controls. *Choi et al.* [2007] pointed to the existence of the effect in various observational data with no further interpretations. Differentiating from previous research, this study focused on the soil water contained between the soil and impermeable bedrock surfaces (1 m depth) at the fairly fine temporal resolution (1 day). This allowed the space-time integration of the effects of the full set of simulated hydrological processes and thus lead to explicit mechanistic inferences on causes of soil water spatial variability.

[43] It should be further emphasized here that the key reasons leading to the observed hysteretic patterns of soil moisture heterogeneity are the imposed conditions of soil with high conductivity and regular shallow bedrock that replicates surface topography. Both are the design characteristics of hillslopes to be constructed in the Biosphere 2 facility [*Hopp et al.*, 2009]. The explanation (see the discussion in 3.2) is that (1) while infiltration fronts from some storms become impeded at shallow depths and, ultimately, depleted by the evapotranspiration process, and (2) for certain wetting conditions, the high saturated hydraulic conductivity allows for rapid percolation of event moisture down to the impervious bottom, resulting in saturated (or nearly-saturated) conditions that lead to efficient subsurface exchange. As the study argues, the outcomes (1) and (2) strongly depend on the initial conditions of the catchment, characterized by both moisture mean and variability.

[44] The existence of the attractor in the phase space of the system may also represent a hypothetically interesting case when interactions between hydrological and vegetation systems are considered. Note the cases with the initialization states that suppress subsurface moisture exchange for any imposed rainfall event (e.g., $\overline{\theta}_{ini}$ = 0.0742, 0.0843 in section 3.2.1). They may be argued to represent a potentially significant effect of land surface conditions on the function of vegetation system and even on climate. For example, when the land surface dries out beyond a certain threshold, vegetation transits to a stressed state with a significant loss of foliage. Plants may entirely die out in most of the landscape area, except, possibly, narrow riparian areas that are fed by moisture from shallow surficial aquifers. Subsequent precipitation events will be unable to "knock out" the system from the attractor space to the dynamics mode that exhibits a temporary formation of the phreatic zone. This will prevent efficient subsurface moisture redistribution and formation of wetter near-channel corridors that would otherwise persist over longer periods of time, sustaining remaining vegeta-

tion. A complete mortality of vegetation may thus become one possible scenario with low likelihood of seedling re-establishment, even if favorable climatic conditions return. Note though that in the light of the previous discussion, dead vegetation in most of the landscape would mimic bare soil conditions that are argued to be more conducive to subsurface lateral moisture redistribution (when integrated over the long-term). The net implication is likely to be to the effect of the outcome presented in the above discussion but the question certainly requires more research. Further, while highly speculative and model resolution-dependent, recent studies point to the overall significance of the role of coupled groundwater-vegetation dynamics in the overlying atmosphere [e.g., *Maxwell and Kollet*, 2008; *Jiang et al.*, 2009].

[45] Another key finding of the study is the long-term effect of vegetation function that appears to exert a "homogenizing" effect on domain soil moisture. This conclusion is in agreement with the earlier analysis by *Teuling and Troch* [2005], who employed a simpler, quasi-spatial model of hydrological budget. The effect is not sensitive to vegetation initialization over the timescales considered. For example, one could argue that when initial biomass pools are not representative of a given climate and/or terrain location, vegetation would evolve in highly transient conditions; the overall outcome might then contribute to the identified "homogenizing" effect. The insensitivity of the effect to initialization has been confirmed by simulations with 22-year long spin-up period and simulation with initial conditions where spatially-distributed long-term averages of carbon pools were used.

[46] Since this modeling study focused on a particular climate regime and assumed a somewhat idealized representation of the zero-order catchment, a discussion is warranted on whether the analyses presented here would be valid under different sets of constraints/forcings. In conditions of deeper and/or irregular bedrock surface, as is the case for most natural systems [e.g., *Freer et al.*, 2002; *McGlynn et al.*, 2002; *Tromp-van Meerveld and McDonnell*, 2006], the presented analysis will become more complex but not irrelevant. It will likely have to include additional constraints that impose control on triggering the subsurface exchange, such as the characteristics of moisture retention in local bedrock depressions. Furthermore, a "leaky" bedrock boundary condition could exert a substantial, if not dominant, control on hydrological response in catchments [e.g., *Hooper*, 2003; *Tromp-van Meerveld and Weiler*, 2008]. However, there is ample in situ evidence of occurrence of subsurface flow above the bedrock-soil interface [e.g., *Dunne and Black*, 1970a, 1970b; *Weyman*, 1970a, 1970b; *Wilson et al.*, 1990] that has been argued to contribute significantly to the evolution of soil moisture heterogeneity in this study.

[47] Field observations show that the soil hydraulic properties may vary significantly in space even within a given soil type [e.g., *Warrick and Nielsen*, 1980]. Such spatial variability results in the hydrological response conditioned by the existence of an ensemble of moisture retention curves and hydraulic conductivities, which may exhibit hysteresis and state-dependent anisotropy [e.g., *Yeh et al.*, 1985a, 1985b]. Variability in soil properties is thus sometimes argued to be one of the primary contributors to the spatial heterogeneity of soil moisture [e.g., *Teuling and Troch*, 2005; *Lawrence and Hornberger*, 2007; *Vereecken et al.*, 2007]. Specifically, this has been argued for shallow surface soil moisture, which may be de-coupled from the subsurface flow phenomena (see discussion in 3.1). This study does not address such soil effects and it is difficult to hypothesize what essential implications would be were these effects explicitly introduced. A priori, the major conclusions of this study would hold. However, both the attractor and the phase spaces would exhibit a larger range of spatial variability of θ, i.e., larger magnitudes of $C_v(\bar{\theta})$ in Figure 1b, because of the superposition of the "deterministic" effects of physical mechanisms and "random" effects of soil texture spatial variability.

[48] The discussed patterns are reproduced for a semiarid environment, where energy excess leads to quick drying, i.e., rapid return of perturbed system to the attractor space. A priori, assuming the same physical constraints in the domain, wetter climates should yield a wider range of magnitudes in the $C_v(\bar{\theta})$ pattern, possibly making the relationship even more complex. The reason is that in conditions of larger perturbations and smaller potential evapotranspiration, a system would less frequently reach the attractor space. As discussed earlier, the latter is predominantly determined by the topographic signature of the domain and spatial differences in energy inputs and standing biomass. It should be remembered, however, that the discussion has concerned the moisture content integrated over the entire depth of the soil profile. If empirical observations do not extend to the depths at which the periodic influence of the saturated dynamics on spatial variability becomes pronounced, or the observational period is too short, the analyzed effects will unlikely be fully present in empirical data.

[49] On the final note, the study has demonstrated the non-uniqueness of system response for the same initial mean state relative to forcing, i.e., precipitation events of different magnitudes. In an alternative approach, not explicitly discussed here, one could argue that the system could exhibit a non-uniqueness of response to the same forcing for the same initial mean states. The difference is that the latter would be characterized by varying degrees of soil moisture spatial heterogeneity. This is not typically considered in the hydrological analysis, as the mean state is implicitly assumed to fully define the initial state of the system [e.g., *Noto et al.*, 2008]. The existence of the attractor space and the fact that a large perturbation may temporarily deviate the evolution of the system away from the attractor space both point to the significance of system memory in hydrological analysis. Such memory effects directly translate into the non-uniqueness of catchment rainfall-runoff process and hydrological predictability, as previously discussed for the storage-runoff relationship by *Beven* [2006]. These features need to be taken into account in studies that attempt to reveal patterns of system dynamics.

[50] **Acknowledgments.** Authors thank two anonymous reviewers and Enrique Vivoni for their constructive comments. Authors would like to thank the participants of the Biosphere 2 Hillslope Experiment planning workshops for constructive discussions of the study and the B2 Earth Science Steering Committee for the support of this work. Authors also personally thank Murugesu Sivapalan for inspiring this study and a partial support by the NSF-funded Hydrologic Synthesis Project at the University of Illinois at Urbana-Champaign. This work was supported by NSF grant 0911444. G. D. Jenerette was supported by NSF grant 0916069. Help of Vineet Yadav in the statistical analysis of simulation results is gratefully acknowledged.

The technical support of the Center for Advanced Computing at the University of Michigan is also acknowledged.

References

Albertson, J. D., and N. Montaldo (2003), Temporal dynamics of soil moisture variability: 1. Theoretical basis, *Water Resour. Res.*, *39*(10), 1274, doi:10.1029/2002WR001616.

Beven, K. J. (2006), Searching for the holy grail of scientific hydrology: $Q_t = H(\vec{S},\vec{R}, \Delta t)A$ as closure, *Hydrol. Earth Syst. Sci.*, *10*, 609–618.

Bisht, G., U. Narayan, and R. L. Bras (2008), Prediction of seasonal to inter-annual hydro-climatology including the effects of vegetation dynamics and topography over large river basins, *Eos Trans. AGU*, *89*(53), Fall Meet. Suppl., Abstract H23G-02.

Carsel, R. F., and R. S. Parrish (1988), Developing joint probability-distributions of soil-water retention characteristics, *Water Resour. Res.*, *24*(5), 755–769.

Celia, M., E. Bouloutas, and R. Zarba (1990), A general mass-conservative numerical solution for the unsaturated flow equation, *Water Resour. Res.*, *26*(7), 1483–1496.

Choi, M., and J. M. Jacobs (2007), Soil moisture variability of root zone profiles within SMEX02 remote sensing footprints, *Adv. Water Resour.*, *30*(4), 883–896, doi:10.1016/j.advwatres.2006.07.007.

Choi, M., J. M. Jacobs, and M. H. Cosh (2007), Scaled spatial variability of soil moisture fields, *Geophys. Res. Lett.*, *34*, L01401, doi:10.1029/2006GL028247.

Cosh, M. H., J. R. Stedinger, and W. Brutsaert (2004), Variability of surface soil moisture at the watershed scale, *Water Resour. Res.*, *40*, W12513, doi:10.1029/2004WR003487.

Cosh, M., T. Jackson, S. Moran, and R. Bindlish (2008), Temporal persistence and stability of surface soil moisture in a semi-arid watershed, *Remote Sens. Environ.*, *112*(2), 304–313.

Cox, J., G. W. Fraiser, and K. G. Renard (1986), Biomass distribution at grassland and shrubland sites, *Rangelands*, *8*(2), 67–68.

Dontsova, K., C. I. Steefel, S. Desilets, A. Thompson, and J. Chorover (2009), Solid phase evolution in the Biosphere 2 hillslope experiment as predicted by modeling of hydrologic and geochemical fluxes, *Hydrol. Earth Syst. Sci.*, *13*(12), 2273–2286.

Dunne, T., and R. Black (1970a), An experimental investigation of runoff production in permeable soils, *Water Resour. Res.*, *6*(2), 478–490.

Dunne, T., and R. Black (1970b), Partial area contributions to storm runoff in a small New England watershed, *Water Resour. Res.*, *6*(5), 1296–1311.

Emmerich, W. E., and C. L. Verdugo (2008), Long-term carbon dioxide and water flux database, Walnut Gulch Experimental Watershed, Arizona, United States, *Water Resour. Res.*, *44*, W05S09, doi:10.1029/2006WR005693.

Entekhabi, D., and I. Rodriguez-Iturbe (1994), Analytical framework for the characterization of the space-time variability of soil moisture, *Adv. Water Resour.*, *17*, 35–45.

Erickson, T., M. Williams, and A. Winstral (2005), Persistence of topographic controls on the spatial distribution of snow in rugged mountain terrain, Colorado, United States, *Water Resour. Res.*, *41*, W04014, doi:10.1029/2003WR002973.

Famiglietti, J. S., J. A. Devereaux, C. Laymon, T. Tsegaye, P. R. Houser, T. J. Jackson, S. T. Graham, M. Rodell, and P. J. van Oevelen (1999), Ground-based investigation of soil moisture variability within remote sensing footprints during Southern Great Plains 1997 (SGP97) Hydrology Experiment, *Water Resour. Res.*, *35*(6), 1839–1851.

Famiglietti, J. S., D. Ryu, A. A. Berg, M. Rodell, and T. J. Jackson (2008), Field observations of soil moisture variability across scales, *Water Resour. Res.*, *44*, W01423, doi:10.1029/2006WR005804.

Freer, J., J. J. McDonnell, K. J. Beven, N. E. Peters, D. A. Burns, R. P. Hooper, B. Aulenbach, and C. Kendall (2002), The role of bedrock topography on subsurface storm flow, *Water Resour. Res.*, *38*(12), 1269, doi:10.1029/2001WR000872.

Friend, A., A. Stevens, R. Knox, and M. Cannell (1997), A process-based, terrestrial biosphere model of ecosystem dynamics (Hybrid v3.0), *Ecol. Modell.*, *95*(2–3), 249–287.

Grayson, R. B., A. W. Western, F. H. S. Chiew, and G. Blöschl (1997), Preferred states in spatial soil moisture patterns: Local and nonlocal controls, *Water Resour. Res.*, *33*(12), 2897–2908.

Guswa, A. J. (2005), Soil moisture limits on plant uptake: An upscaled relationship for water-limited ecosystems, Adv. *Water Resour.*, *28*(6), 543–552.

Guswa, A. J., M. A. Celia, and I. Rodriguez-Iturbe (2002), Models of soil moisture dynamics in ecohydrology: A comparative study, *Water Resour. Res.*, *38*(9), 1166, doi:10.1029/2001WR000826.

Gutiérrez-Jurado, H. A., E. R. Vivoni, J. B. J. Harrison, and H. Guan (2006), Ecohydrology of root zone water fluxes and soil development in complex semiarid rangelands, *Hydrol. Processes*, *20*, 3289–3316.

Hillel, D. (1980), *Fundamentals of Soil Physics*, 413 pp., Academic, New York.

Hooper, R. P. (2003), Diagnostic tools for mixing models of stream water chemistry, *Water Resour. Res.*, *39*(3), 1055, doi:10.1029/2002WR001528.

Hopp, L., C. Harman, S. Desilets, C. Graham, J. McDonnell, and P. A. Troch (2009), Hillslope hydrology under glass: Confronting fundamental questions of soil-water-biota co-evolution at Biosphere 2, *Hydrol. Earth System Sciences*, *13*(11), 2105–2118.

Huxman, T., P. Troch, J. Chorover, D. D. Breshears, S. Saleska, J. Pelletier, X. Zeng, and J. Espeleta (2009), The hills are alive: Earth science in a controlled environment, *Eos Trans. AGU*, *34*(90), 120.

Ivanov, V. Y., R. L. Bras, and E. R. Vivoni (2008a), Vegetation-hydrology dynamics in complex terrain of semiarid areas: 1. A mechanistic approach to modeling dynamic feedbacks, *Water Resour. Res.*, *44*, W03429, doi:10.1029/2006WR005588.

Ivanov, V. Y., R. L. Bras, and E. R. Vivoni (2008b), Vegetation-hydrology dynamics in complex terrain of semiarid areas: 2. Energy-water controls of vegetation spatiotemporal dynamics and topographic niches of favorability, *Water Resour. Res.*, *44*, W03430, doi:10.1029/2006WR005595.

Ivanov, V. Y., R. L. Bras, and E. R. Vivoni (2008c), Ecohydrologic dynamics in areas of complex topography in semiarid ecosystems, *Eos Trans. AGU*, *89*(53), Fall Meet. Suppl., Abstract H23G-06.

Jackson, R., J. Canadell, J. Ehleringer, H. Mooney, O. Sala, and E. Schulze (1996), A global analysis of root distributions for terrestrial biomes, *Oecologia*, *108*(3), 389–411.

Jayawardena, A., and F. Lai (1994), Analysis and prediction of chaos in rainfall and streamflow time series, *J. Hydrol.*, *153*(1–4), 23–52.

Jiang, X. Y., G. Y. Niu, and Z. L. Yang (2009), Impacts of vegetation and groundwater dynamics on warm season precipitation over the central United States, *J. Geophys. Res.*, *114*, D06109, doi:10.1029/2008JD010756.

Keefer, T. O., M. S. Moran, and G. B. Paige (2008), Long-term meteorological and soil hydrology database, Walnut Gulch Experimental Watershed, Arizona, United States, *Water Resour. Res.*, *44*, W05S07, doi:10.1029/2006WR005702.

Krasnosel'skii, M. A., and A. V. Pokrovskii (1989), *Systems With Hysteresis*, Springer, New York.

Kumar, P. (2004), Layer averaged Richard's equation with lateral flow, *Adv. Water Resour.*, *27*(7), 522–532, doi:10.1016/j.advwatres.2004.02.007.

Lawrence, J. E., and G. M. Hornberger (2007), Soil moisture variability across climate zones, *Geophys. Res. Lett.*, *34*, L20402, doi:10.1029/2007GL031382.

Leuning, R. (1995), A critical appraisal of a combined stomatal-photosynthesis model for C3 plants, *Plant Cell Environ.*, *18*, 357–364.

Mascart, P., J. Noilhan, and H. Giordani (1995), A modified parameterization of flux-profile relationships in the surface layer using different roughness length values for heat and momentum, *Boundary Layer Meteorol.*, *72*, 331–334.

Maxwell, R. M., and S. J. Kollet (2008), Interdependence of groundwater dynamics and land-energy feedbacks under climate change, *Nat. Geosci.*, *1*(10), 665–669, doi:10.1038/ngeo315.

McDonnell, J. J. (2003), Where does water go when it rains? Moving beyond the variable source area concept of rainfall-runoff response, *Hydrol. Processes*, *17*, 1869–1875, doi:10.1002/hyp.5132.

McGlynn, B. L., J. J. McDonnel, and D. D. Brammer (2002), A review of the evolving perceptual model of hillslope flowpaths at the Maimai catchments, New Zealand, *J. Hydrol.*, *257*(1–4), 1–26.

Noto, L. V., V. Y. Ivanov, R. L. Bras, and E. R. Vivoni (2008), Effects of initialization on response of a fully-distributed hydrologic model, *J. Hydrol.*, *352*, 107–125, doi:10.1016/j.jhydrol.2007.12.031.

Noy-Meir, I. (1973), Desert ecosystems: Environment and producers, *Annu. Rev. Ecol. Syst.*, *4*, 25–51.

Pockman, W., and J. Sperry (2000), Vulnerability to xylem cavitation and the distribution of Sonoran desert vegetation, *Am. J. Bot.*, *87*(9), 1287–1299.

Raftery, A. (1995), Bayesian model selection in social research, *Sociol. Methodol.*, *25*, 111–163.

Renard, K. G., M. H. Nichols, D. A. Woolhiser, and H. B. Osborn (2008), A brief background on the U.S. Department of Agriculture Agricultural

Research Service Walnut Gulch Experimental Watershed, *Water Resour. Res.*, *44*, W05S02, doi:10.1029/2006WR005691.

Schwarz, G. (1978), Estimating dimension of a model, *Ann. Stat.*, *6*, 461–464.

Scott, R. L., W. J. Shuttleworth, T. O. Keefer, and A. W. Warrick (2000), Modeling multiyear observations of soil moisture recharge in the semiarid American Southwest, *Water Resour. Res.*, *36*, 2233–2247.

Sivandran, G., G. Bisht, V. Y. Ivanov, and R. L. Bras (2008), An eleven-year validation of a physically-based distributed dynamic ecohydroloswgical model tRIBS+VEGGIE: Walnut Gulch Experimental Watershed, *Eos Trans. AGU*, *89*(53), Fall Meet. Suppl., Abstract H21F-0888.

Teuling, A. J., and P. A. Troch (2005), Improved understanding of soil moisture variability dynamics, *Geophys. Res. Lett.*, *32*, L05404, doi:10.1029/2004GL021935.

Teuling, A. J., F. Hupet, R. Uijlenhoet, and P. A. Troch (2007), Climate variability effects on spatial soil moisture dynamics, *Geophys. Res. Lett.*, *34*, L06406, doi:10.1029/2006GL029080.

Troch, P. A., C. Paniconi, and E. E. vanLoon (2003), Hillslope-storage Boussinesq model for subsurface flow and variable source areas along complex hillslopes: 1. Formulation and characteristic response, *Water Resour. Res.*, *39*(11) 1316, doi:10.1029/2002WR001728.

Tromp-van Meerveld, H. J., and J. J. McDonnell (2006), On the interrelations between topography, soil depth, soil moisture, transpiration rates and species distribution at the hillslope scale, *Adv. Water Resour.*, *29*, 293–310, doi:10.1016/j.advwatres.2005.02.016.

Tromp-van Meerveld, I., and M. Weiler (2008), Hillslope dynamics modeled with increasing complexity, *J. Hydrol.*, *361*, 24–40, doi:10.1016/j.jhydrol.2008.07.019.

Tsuboyama, Y., R. C. Sidle, S. Noguchi, S. Murakami, and T. Shimizu (2000), A zero-order basin—Its contribution to catchment hydrology and internal hydrological processes, *Hydrol. Processes*, *14*(2), 387–401.

van Genuchten, M. T. (1980), A closed-form equation for predicting the hydraulic conductivity of unsaturated soils, *Soil Sci. Soc. Am. J.*, *44*, 892–898.

Vereecken, H., T. Kamai, T. Harter, R. Kasteel, J. Hopmans, and J. Vanderborght (2007), Explaining soil moisture variability as a function of mean soil moisture: A stochastic unsaturated flow perspective, *Geophys. Res. Lett.*, *34*, L22402, doi:10.1029/2007GL031813.

Vivoni, E., M. Gebremichael, C. Watts, R. Bindlish, and T. Jackson (2008), Comparison of ground-based and remotely-sensed surface soil moisture estimates over complex terrain during SMEX04, *Remote Sens. Environ.*, *112*(2), 314–325.

Vivoni, E. R., J. C. Rodrguez, and C. J. Watts (2010), On the spatiotemporal variability of soil moisture and evapotranspiration in a mountainous basin within the North American monsoon region, *Water Resour. Res.*, *46*, W02509, doi:10.1029/2009WR008240.

Warrick, A. W., and D. R. Nielsen (1980), Spatial variability of soil physical properties in the field, in *Applications of Soil Physics*, edited by D. Hillel, pp. 319–344, Academic, New York.

Weiler, M., and J. J. McDonnell (2004), Virtual experiments: A new approach for improving process conceptualization in hillslope hydrology, *J. Hydrol.*, *285*, 3–18, doi:10.1016/S0022-1694(03)00271-3.

Western, A., S. Zhou, R. Grayson, T. McMahon, G. Blöschl, and D. Wilson (2004), Spatial correlation of soil moisture in small catchments and its relation to dominant spatial hydrological processes, *J. Hydrol.*, *286*, 113–134.

Weyman, D. (1970a), Throughflow on hillslopes and its relation to the stream hydrograph, *Bull. Int. Assoc. Sci. Hydrol.*, *15*(2), 25–33.

Weyman, D. (1970b), Measurements of the downslope flow of water in a soil, *J. Hydrol.*, *20*, 267–288.

Wilson, G. V., P. M. Jardine, R. J. Luxmoore, and J. R. Jones (1990), Hydrology of a forested hillslope during storm events, *Geoderma*, *46*, 119–138.

Yeh, T.-C. J., L. Gelhar, and A. Gutjahr (1985a), Stochastic analysis of unsaturated flow in heterogeneous soils: 1. Statistically isotropic media, *Water Resour. Res.*, *21*(4), 447–456.

Yeh, T.-C. J., L. Gelhar, and A. Gutjahr (1985b), Stochastic analysis of unsaturated flow in heterogeneous soils: 2. Statistically anisotropic media, *Water Resour. Res.*, *21*(4), 457–464.

J. F. Espeleta, Biosphere 2, University of Arizona, Tucson, AZ 85721, USA.

S. Fatichi, Department of Civil and Environmental Engineering, University of Florence, Via S. Marta, 3, I-50139 Florence, Italy.

T. E. Huxman, Department of Ecology and Evolutionary Biology, University of Arizona, Tucson, AZ 85721, USA.

V. Y. Ivanov, Department of Civil and Environmental Engineering, University of Michigan, Ann Arbor, MI 48109-2125, USA. (ivanov@umich.edu)

G. D. Jenerette, Department of Botany and Plant Sciences, University of California, 2150 Batchelor Hall, Riverside, CA 92521-0124, USA.

P. A. Troch, Department of Hydrology and Water Resources, University of Arizona, 1133 E. James E. Rogers Way, Tucson, AZ 85721, USA.